Biomedical Engineering Letters (2020) 10:481–492
https://doi.org/10.1007/s13534-020-00172-7

REVIEW ARTICLE

Recent additive manufacturing methods categorized by characteristics of ceramic slurries for producing dual-scale porous ceramics

Woo-Youl Maeng[1] · **Hyun Lee**[1]

Received: 15 July 2020 / Revised: 4 September 2020 / Accepted: 21 September 2020 / Published online: 1 October 2020

Abstract
Porous ceramics have been utilized in various fields due to their advantages derived from characteristics of ceramics and porous structure and they were produced by versatile fabricating methods. However, the adoption of differently scaled pores in the porous ceramics by conventional pore forming strategies which results in dual-scale porosity has been studied to combine the specific functional abilities of each scaled pore. Those proposed strategies were supplemented to the recent additive manufacturing methods for constructing complicated structure with precisely controlled fabricating conditions. In this review, we provide the researches creating dual-scale porous ceramics with additive manufacturing which utilized the ceramic slurries containing homogeneous solution of photocurable monomers and terpenes. Introduction of the basic way to prepare photocurable monomer and terpene incorporated ceramic slurries which are suitable for specific printing mechanism was firstly discussed. And based on the characteristics of slurries, lithography-based and extrusion-based method are discussed with the experimental results. Subsequently, the remaining challenges of the techniques are further discussed with suggesting potentially capable approaches to overcome the limitations.

Keywords Dual-scale porous ceramics · Additive manufacturing · Slurry characteristics · Lithography · Extrusion

1 Introduction

Porous ceramics are ceramics containing 15–90 vol% of pores which are characterized by advantages of ceramics (high mechanical properties, excellent thermal stability and corrosion resistance) and pores (extended surface area, roughened surface) [1–5]. These porous ceramics have been extensively utilized as insulator, electrode for battery and fuel cells, and biological applications. As electronic and thermal utilization, pores facilitate charge (electrons and ions) transport and disturb the heat transfer by trapped air inside pores [6, 7]. 3D bilayered solid-state electrolyte framework for high energy density lithium metal-sulfur batteries were produced via tape-casting method by Fu et al. [8]. They employed polymethylmethacrylate (PMMA) bead for generating pores inside the thick garnet layer which can host the electrode material and liquid electrolyte. And application of that resulted in high sulfur loading, coulombic efficiency. As a way to reduce thermal conductivity, Han et al. investigated the effect of porosity to thermal conductivity of porous mullite ceramics [9]. Porous mullite ceramics prepared by combined gel-casting and microwave heating method exhibited pores with several hundreds of μm. And thermal conductivity of the products was inversely proportional to the porosity. Regarding biological applications, pores with diverse range of size have been known to possess distinctive roles for enhancing tissue regeneration around the scaffolds [10–12]. Li et al. proposed a hot-dog like structure combining rods with micro-scale pores inside macro porous hollow tube. The generated hierarchical lamellar porous structure was attributed to the highly promoted formation of new bone [13]. More specific classification to the functions of pores with different sizes were suggested by Sánchez et al. that macro pores within 300–400 μm induces bone ingrowth, vascularization, nutrient transfer, and cell growth [11]. Meanwhile, pores including 1–20 μm distinctively act for cell attraction, cellular development, and directionality of cells [11].

✉ Hyun Lee
leeh0520@korea.ac.kr

[1] Institute of Global Health Technology Research, Korea University, Seoul 02841, Republic of Korea

One of the representative manufacturing methods for porous ceramics with micro-scale pores is utilizing ceramic powder incorporated slurries which containing pore forming agents. In terms of pore forming agents, sacrificial materials which are easily removable at green body state by a simple procedure and which could be eliminated during pyrolysis and sintering have been widely employed. For the former, freeze casting method is generally used and pores are created by rejection of ceramic particles during solidification of freezing vehicles. Since freeze casting is based on the slurries, pore characteristics such as porosity, pore size, and pore shape can easily be tailored by controlling freezing conditions and freezing vehicle. Water, camphene (a kind of terpenes), and tertiary butyl alcohol (TBA) are the most widely incorporated freezing vehicles for freeze casting of porous ceramics. Since they possess different physicochemical characteristics, conducted studies followed their specific conditions for specific porous structures [14–22]. Additionally, customized shapes are also possible through different condition where freezing procedure occurs [23, 24]. Regarding the elimination of pore forming agent during heat treatments, versatile studies reported facilitation of polymeric spheres or beads as pore generators with their particular sizes [25–27]. These polymeric sphere and bead based porous ceramics were distinguished by the pore shape and relatively narrow range of pore size resulted from the source of polymer.

Lately, the advent of various additive manufacturing methods inspired the adoption of pore forming agents to produce porous ceramic scaffolds. Unlike the traditional above-mentioned methods for fabricating porous ceramic scaffolds, additive manufacturing methods are advantageous in facilitating precisely designed structure with interconnected macro-scale pores. Especially, extrusion-based 3D printing methods including ink-jet printing [28, 29], robocasting [30–32], rapid direct deposition of ceramic paste [33], and extrusion free-forming [34, 35] and photopolymerization of ceramic slurries [36, 37] have been developed. In addition to those additive manufacturing techniques, a variety of researches were carried out to generate dual-scale porous ceramics by combining the traditional method utilizing pore forming agents for micro-scale pores and developed additive manufacturing methods for macro-scale pores. Combination of micro-scale pores and macro-scale pores in a single porous ceramic scaffold is characterized by enhanced infiltration and release of fluids or gases, effective volumetric availability, and beneficial to mechanical properties and surface area [38, 39]. Particularly, articles regarding introducing dual-scale pores for biological applications reported that considerable enhancement in tissue regeneration which derived from increased attaching sites for cells [13, 40, 41].

Herein, we introduce recently developed ceramic additive manufacturing methods for dual-scale porous structure utilizing specially designed slurries incorporated with sublimable terpenes. Since terpenes used as pore forming agents generates dendritic pores inside the green bodies during phase transition near the melting temperature and sublimation, micro-scale pores are supplemented in three dimensionally fabricated porous scaffolds. For the first part, preparation of ceramic slurries containing terpenes and photopolymerizable monomers are addressed. And we shall categorize the methods based on the initial phase of the slurries: (1) liquid state slurries adopted in lithography-based 3D printing and (2) solid state slurries used in extrusion-based 3D plotting. Furthermore, potential aspects for advancements of each method are also discussed.

2 Preparation of ceramic slurries containing sublimable terpenes for additive manufacturing

Camphene ($C_{10}H_{16}$) and camphor ($C_{10}H_{16}O$) which are most widely used terpenes for freeze casting method exhibits complete liquid solution state above the melting temperature [42, 43]. And this complete liquid solution become complete solid solution without phase separation even it undergoes cooling procedure at room temperature [42, 43]. Thus, studies regarding freeze casting adopted this camphene/camphor alloy system to generate pores in the ceramic scaffolds by a simple sublimation process. Even though its simplicity and convenience, shape retention ability of green bodies after elimination of camphene and camphor is insufficient to withstand external pressure. Consequently, special care should be taken to the green bodies until the green bodies were put into heat treatment procedure.

As a solution for strengthening of green bodies, photocurable monomers have been supplemented into the ceramic slurries which could hold the initial shape by photopolymerization. However, incorporated photocurable monomers should be dissolved in the slurries since separated photocured polymers are rather detrimental to green body strength. Accordingly, determining the ternary eutectic condition between camphene, camphor, and photocurable monomer for preparing homogeneous ceramic slurries at certain conditions is the most important factor to be applied in ceramic additive manufacturing techniques. As suggested by Tomeckova et al., blended photocurable monomers and camphene/camphor alloy maintain liquid state at a certain range of temperature [43]. In terms of ceramic slurries including the photocurable monomer/camphene/camphor solution, decreasing temperature of the slurries results in solidification of camphene/camphor alloy to be dendritic crystals which induce phase separation from photocurable monomers. Followed photopolymerization of photocurable monomers by ultra violet (UV) radiation fix the dendritic

structure of camphene/camphor alloy and this improves the strength of ceramic green body. Since contained ceramic particles distributed in the photopolymerized parts, removal of camphene/camphor only generated the pores in the scaffolds except the photopolymerized parts.

3 Production of dual-scale porous ceramic scaffolds consisting of macro/micro-scale porous structure

There have been various researches considering dual-scale porous ceramic scaffolds to take advantages of both of macro-scale and micro-scale pores as summarized in Table 1 [44–52]. In particular for monomer/terpene system, thermoreversible behavior of ceramic slurries including photocurable monomer and camphene/camphor alloy near the melting temperature is main factor for determining applicable techniques for ceramic additive manufacturing. Above the melting temperature, the flowability and viscosity of the prepared photocurable ceramic slurries are suitable to be spread on the printing platforms. And this flowability of ceramic slurries is appropriate to be utilized in tape-casting method with supplementation of photocuring equipment which enables lithography-based additive manufacturing since tape-casting requires repetition of spreading ceramic slurries on the platform and laminating the layers [53, 54]. On the other hand, ceramic slurries stored under the melting temperature become soft solid state without any flowability. For this case, extrusion-based 3D additive manufacturing methods should be utilized to produce 3-dimensional ceramic scaffolds by imposing pressure to the frozen feedstocks to be deposited in a certain shape through connected nozzle [55, 56].

3.1 Lithography-based additive manufacturing with tape-casting using molten terpene slurries

Lithography-based additive manufacturing utilizes projection of light to the slurries with specifically designed structure and sequential tape-casting procedure to fabricate desired scaffolds. Compared to other additive manufacturing techniques, degree of precision in printing is superior since photopolymerization occurs only in the parts with light irradiation. And creation of complicated structure such as triply periodic minimal surface (TPMS) structure and customized structure is also possible to be achieved [57, 58]. And the temperature of platform and recoater where ceramic slurries encounter during printing should be controlled to spread ceramic slurries into a thin layer and to hinder unwanted freezing of ceramic slurries. After a single layer is formed, temperature of the platform decreases under the freezing point of the ceramic slurry to induce solidification of terpenes followed by phase separation between monomer and terpenes. Subsequently, UV light irradiation according to 2-dimensionally partitioned images of 3D structure on the layer is conducted to fabricate green framework for layer by layer stacking.

Crucial points for lithography-based ceramic additive manufacturing are determination of temperature for formation of thin ceramic layer, dwelling time for sufficient dendritic growth of terpenes inside the layer, and photocuring time for adhesion between layers. Temperature for building ceramic layer with terpene crystals is generally set by the results of differential scanning calorimetry (DSC). Any specific theoretical calculation or guideline for deciding dwelling time for terpene dendritic growth and photocuring time could not be established due to numerous variables including components of the slurries (photocurable monomer, terpenes, and ceramic powder) and specification of light source (wavelength and power). Thus, related researches determined the detailed fabricating conditions through series of experiments.

Lee et al. fabricated hierarchical porous calcium phosphate (CaP) scaffolds via combination of freeze-casting method and newly developed digital light processing (DLP) system [51]. They utilized camphene and camphor with weight ratio of 2:1 as a freezing vehicle for generating micro-scale pores in the CaP scaffolds. And diurethane

Table 1 Summary of additive manufacturing techniques to fabricate dual-scale porous ceramics [44–52]

Techniques	Characteristics	Reference
UV curing-assisted 3D plotting	Incorporation of photocurable monomer and terpene in the filament	[44]
Direct foam writing/Direct ink writing	Extrusion of particle stabilized foam with trapped air bubbles or pore formers 3-dimensionally designed macro-scale pores with micro-scale pores	[45–47]
Powder based 3D printing	Injection of printing liquid on the mixture of polymer, active filler, and inactive filler Controlled pore characteristics based on the amount of fillers	[48]
Camphene/ceramic co-extrusion	Using camphene as a pore former in core and shell parts Unidirectional macrochannel with interconnected pore walls	[49, 50]
Digital light processing	Tape-casting of photopolymerizable ceramic slurry containing freezing vehicles Creating highly complex shape with excellent precision	[51, 52]

dimethacrylate (UDMA) and phenylbis(2,4,6-trimethylbonzoyl)phosphine oxide (PPO) were used as photocurable monomer and photoinitiator for photopolymerization of each layer. All of the ingredients for photocurable ceramic slurries were homogeneously mixed without phase separation at 70 °C. Custom-built DLP equipment with digital micromirror device (DMD) and temperature controller to platform and recoater was set to piling up thin layer of prepared ceramic slurries (Fig. 1).

Thermal behavior of the slurries containing different amounts of freezing vehicles (camphene and camphor) was monitored by DSC analysis to determine the temperature of platform to induce dendritic growth of freezing vehicles. According to the article, solidifying temperature of the slurries increased as increasing the content of freezing vehicle which were monitored as ~ 35 °C for 40 vol% of terpenes to ~ 51 °C for 60 vol% of terpenes. This phenomenon was derived from declined heat conductivity induced by incorporated UDMA and CaP particles. Following the obtained results, temperature of platform was differently controlled at each condition to fully solidify the terpenes.

Evolution of terpene dendritic crystals in the layer and photopolymerization process sequentially take place right after spreading the ceramic slurries on the platform. After even spreading of ceramic slurries, temperature of the platform is decreased until the programmed value. While descending the temperature, dendritic growth of freezing vehicles and phase separation occurs with repelling monomer and ceramic particles. Certain range of dwelling time is inserted for solidification and photopolymerization procedure by UV irradiation. Regarding photopolymerization of photocurable monomer, a trend of cure-depth and curing

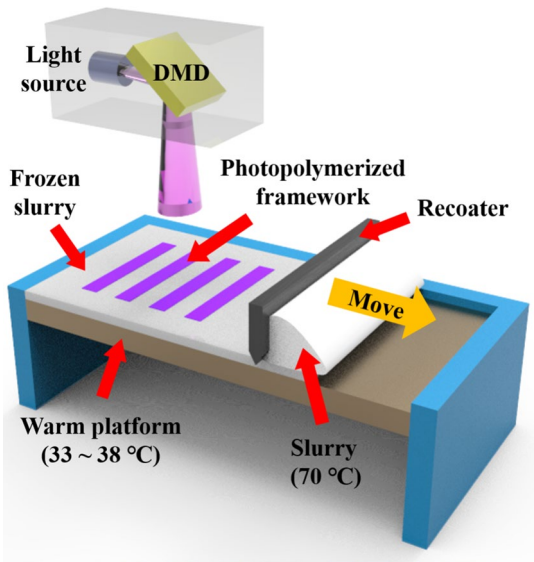

Fig. 1 Custom-built DLP equipment for fabricating dual-scale porous CaP scaffolds

time should be analyzed to acquire optimal condition with sufficient interfacial bonding between the layers. Increased exposure time resulted in thicker photopolymerized layer without significant differences regarding to other variables such as porosity. Based on the identified relationship between exposure time and thickness of photopolymerized layer, the authors adopted 220 μm thickness with 20 s of curing time. The reason for choosing 220 μm thickness which was thinner than the photocured thickness at 20 s of curing time was to acquire sufficient strength of green body and bonding between the layers by adequate percent conversion of UDMA [59].

Wood-pile structured macro-scale pores were adopted according to initial design with identical porosity of 50 vol% as demonstrated in Fig. 2a-c. However, measured overall porosity of scaffolds with 40 vol%, 50 vol%, and 60 vol% of freezing vehicles were 61 ± 2 vol%, 66 ± 2 vol%, and 70 ± 1 vol%, respectively. And the measured microporosity which resulted in higher overall porosity following increased freezing vehicle contents was 27–53 vol% with increased freezing vehicle contents of 40–60 vol%. Comparing overall porosity which theoretical calculated by initial macroporosity and microporosity with that from dimensional calculation, slight difference less than 5 vol% was noted. This difference was attributed to the scattering of projected light due to incorporated ceramic particles and shrinkage during debinding and sintering process. And increment in pore size of micro-scale pores was originated from the higher amount of freezing vehicle contents (Fig. 2d–f).

Further research presented dual-scale porous CaP scaffolds with complicated gyroid structure utilizing identical ceramic slurries and DLP system [52]. Gyroid structure is one of the TPMS structure which possesses fully interconnected pores with a certain degree of curvature [60]. And this structure is extensively studied by a variety of fields since it is a kind of biomimetic structure possessing high degree of structural stiffness and interconnectivity of pores [60, 61]. However, constructing complex gyroid structure has been hard to be achieved by conventional filament-based additive manufacturing techniques due to lack of freedom in printing path. Thus, this research definitely demonstrated the advantage of DLP technique with a wide range of applicable shapes. Figure 3 illustrates the optical images of the CaP scaffolds with different amount of camphene/camphor alloy. Even though the border between the layers were clearly shown, cracks or defects in the scaffolds were not found.

Microstructure of fabricated gyroid CaP scaffolds were analyzed by scanning electron microscopy (SEM). Macro-scale pores between the curved frameworks were established regardless of amount of camphene/camphor alloy (Fig. 4a–c). As demonstrated in Fig. 4d–f, micro-scale pores were generated within a few micrometer by dendritic growth of camphene/camphor alloy which indicates that the

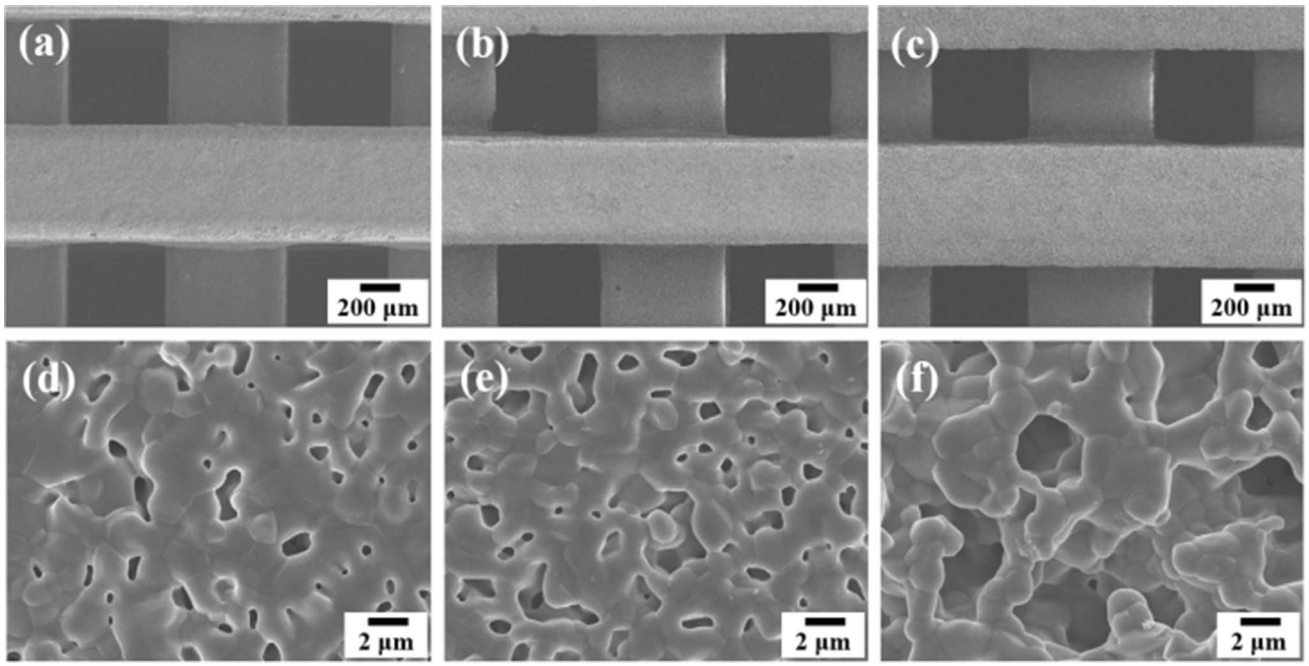

Fig. 2 Structure of macro/micro-scale pores in the CaP frameworks produced by DLP system with **a**, **d** 40 vol%, **b**, **e** 50 vol%, and **c**, **f** 60 vol% of freezing vehicle contents

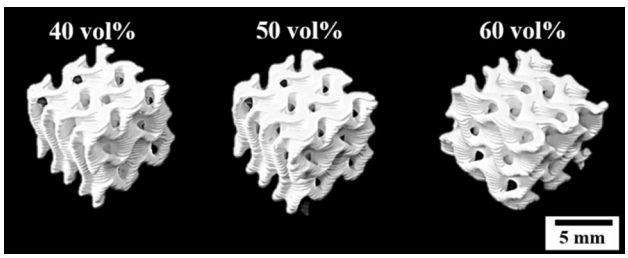

Fig. 3 Optical images of the gyroid CaP scaffolds with 40 vol%, 50 vol%, and 60 vol% of camphene/camphor alloy

scaffolds are consisted of dual-scale pores with macro-scale and micro-scale.

Assessment of the effect of micro-scale pores in the scaffolds was carried out by water penetration capability (Fig. 5). Relatively simple strategy was used to evaluate water penetration capability which based on the fact that micro-scale pores are beneficial to mass transport [62, 63]. Results obtained from water penetration capability test indicated that interconnected micro-scale pores in the CaP framework enhanced the rate of mass transport because the speed of water adsorption from bottom to top was faster in the scaffolds with larger amounts of camphene/camphor alloy. Furthermore, in vitro cell attachment and cell proliferation test using MC3T3-E1 pre-osteoblast cell line (ATCC, CRL-2593, Rockville, MD, USA) were conducted to examine the biocompatibility of the scaffolds. Obtained CLSM images revealed that adhered morphology of cells was similar in all of the dual-scale porous CaP scaffolds as shown in Fig. 6a. Cell proliferation evaluation through monitoring cell number proved improved cell proliferation in the scaffolds with increasing camphene/camphor content (Fig. 6b). Enhanced biocompatibility following the increased camphene/camphor content is mainly due to the increased roughness of the surface by micro-scale pores [64]. This finding suggests that fabricated dual-scale porous CaP scaffolds by DLP process are applicable to hard tissue engineering.

3.2 Photocuring -assisted 3D plotting technique using frozen terpene feedstocks

Unlike the lithography-based additive manufacturing techniques using liquid phase ceramic slurries, extrusion-based manufacturing systems have also been extensively studied which employing solidified ceramic slurries to achieve dual-scale porosity [65, 66]. However, traditional extrusion-based additive manufacturing techniques showed difficulties in producing complex shape, especially for free-standing structure. As extrusion-based plotting utilizes frozen filament to build the scaffold with layer stacking, lack of consolidation of green filament at room temperature requires supplementary supporting parts which should eventually be removed. Noted by that challenges, Maeng et al. proposed photocurable monomer as an enhancer for shape retention ability during plotting 3D structure [44]. They developed UV curing-assisted

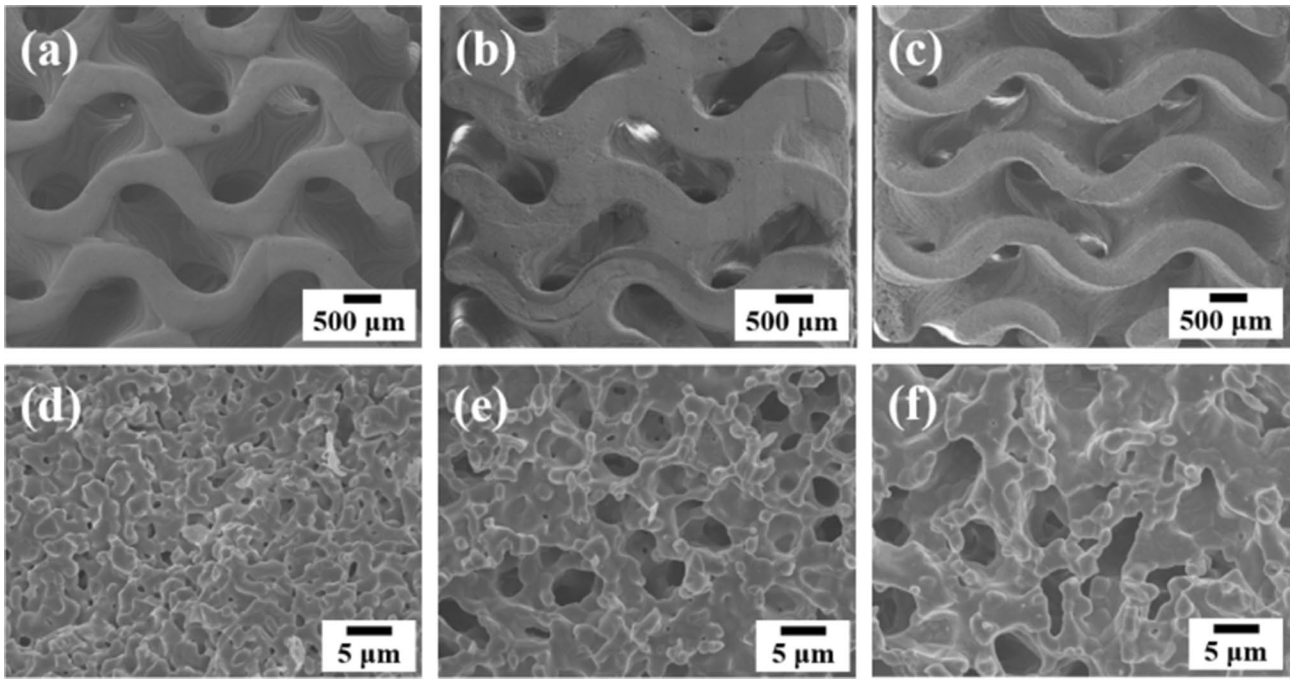

Fig. 4 SEM images of the gyroid CaP scaffolds in terms of incorporating amount of camphene/camphor alloys: **a**, **d** 40 vol%, **b**, **e** 50 vol%, and **c**, **f** 60 vol%. Viewed from the normal **a**–**c** to the building direction and (d-f) high magnification of the frameworks

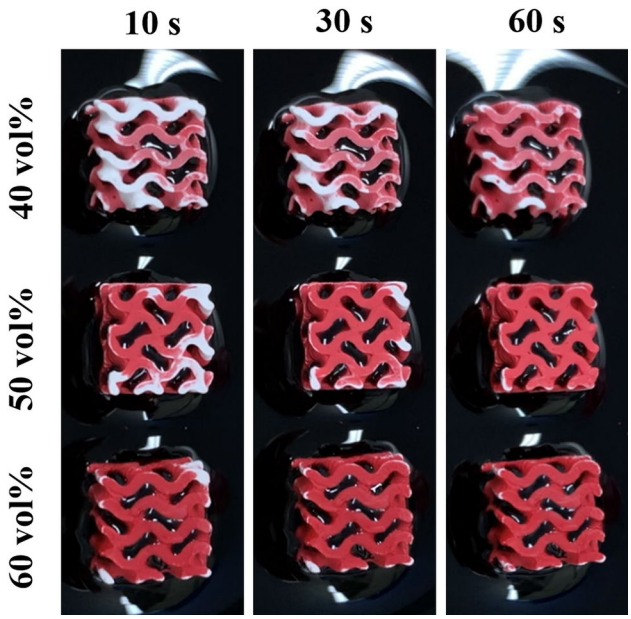

Fig. 5 Water penetration capability assessment of dual-scale porous gyroid CaP scaffolds with different content of freezing vehicles (40 vol%, 50 vol%, and 60 vol%) at 10 s, 30 s, and 60 s of immersion. And red region represents water penetrated part

3D plotting system which induce photopolymerization of the filament right after extrusion from the nozzle. Since the feedrod contains frozen camphene/camphor crystals, sublimation of them would generate micro-scale pores in the filaments. Figure 7 illustrates the schematic diagram of the printing process and set equipment. Sufficiently acquired green filament strength is expected to improve shape retention ability which make possible to create complex structure without any supporting materials.

Identical slurry components suggested in previous works with lithography-based additive manufacturing were utilized [51, 52]. However, the liquid state slurries were frozen at room temperature in the metal mold to generate solid terpene crystals before extrusion. Compressive load and thickness of photocured layer for 50 vol%, 60 vol%, and 70 vol% of terpene contained feedstocks were evaluated to set appropriate plotting process. Trend of compressive load following the displacement were measured using the nozzle with diameter of 500 μm. Monitored behavior of compressive load similar at all of the feedstocks. Compressive load increased until reaching maximum point and maintained at a certain value. The maximum values which reside in 650–2050 N were considered to be suitable for this in situ UV photocuring-assisted 3D plotting system under specific experimental condition. And the photocuring behavior of the feedstock which represented by thickness of photocured layer was assessed by increasing photocuring time (Table 2) [44]. The minimum thickness of photocured layer was 285 ± 6 μm even in the 1 s of UV exposure time which suggested that the use of nozzle with diameter of 500 μm was sufficiently acceptable to fully cure the extruded green filament by irradiated

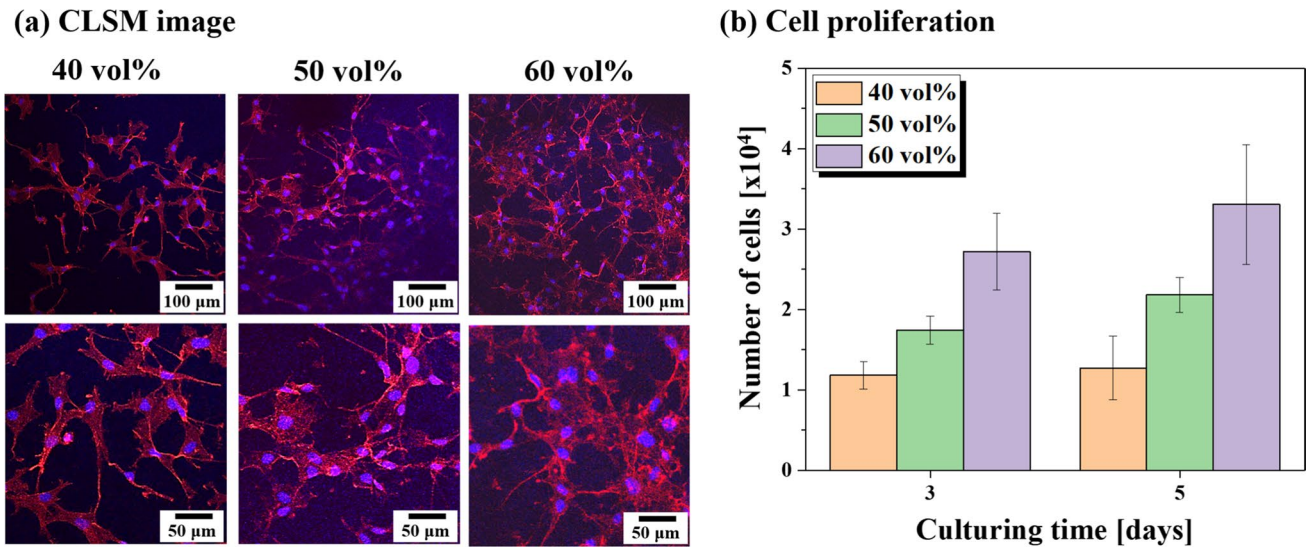

Fig. 6 **a** Representative CLSM images at culturing time of 1 d with low (top) and high (bottom) magnification and **b** monitored cell number after 3 days and 5 days of culturing on the scaffolds

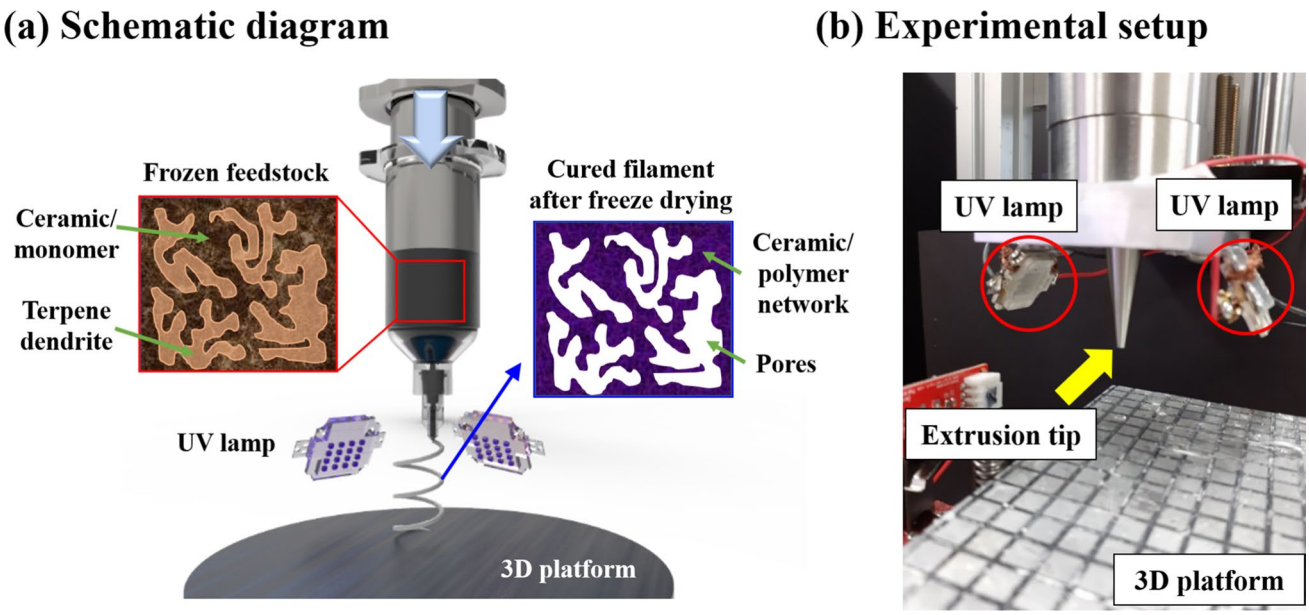

Fig. 7 **a** Schematic diagram of UV curing-assisted 3D plotting system and **b** experimental setup for printing

Table 2 Thickness of photocured layer as a function of curing time for the biphasic calcium phosphate (BCP) feedstocks with different terpene contents [44]

Curing time [s]	1	5	10	15	20	60
Thickness of photo-cured layer [μm]						
50 vol%	285 ± 6	517 ± 6	636 ± 9	720 ± 9	779 ± 14	887 ± 18
60 vol%	302 ± 23	616 ± 8	658 ± 16	860 ± 10	995 ± 7	1134 ± 18
70 vol%	378 ± 7	738 ± 7	817 ± 10	984 ± 23	1115 ± 10	1506 ± 36

UV light from both sides. In all of the experimental groups, thickness of photocured layer increased with decreasing increment ratio as photocuring time increased. The reason for decreasing increment ratio is precedently photopolymerized layer acted as blockage to the additional photocuring of monomers.

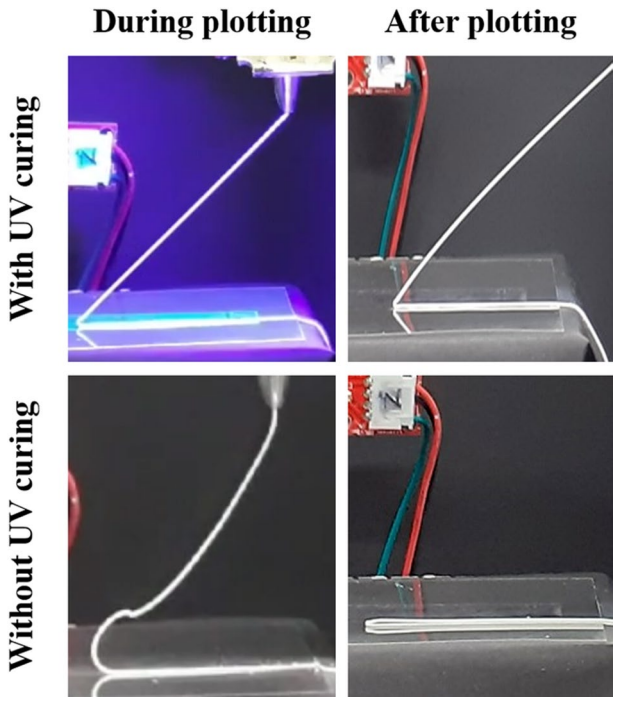

Fig. 8 Optical images of inclined structure fabricated by in situ 3D plotting with and without UV curing process

Additionally, an experiment regarding shape retention ability was conducted comparing the effect of UV exposure. As proposed in Fig. 8, inclined structure was maintained by 3D plotting regardless of application of UV curing during the filament was held by nozzle. On the other hand, remarkable difference was observed right after the end of plotting process where the filament was detached from the nozzle. The green filament which underwent UV curing maintained its initial structure due to photopolymerization of UDMA, whereas green filament without UV curing collapsed. Thus, in situ UV curing-assisted 3D plotting technique possess the potential of generating complex structure without any supporting materials.

The microstructure of the sintered filaments was observed by SEM. As demonstrated in Fig. 9, filaments containing different amounts of terpenes were well fabricated without any deformations (Fig. 9a–c). In higher magnification, the porosity and pore size were slightly changed with increasing terpene amounts (Fig. 9d–f). Actually, quantitatively calculated microporosity were increased from 43% to 70% with increasing 50 vol% and 70 vol% of terpenes, respectively.

Fabrication of dual-scale porous BCP scaffolds by in situ UV curing-assisted 3D plotting was conducted by applying a tool-path with woodpile structure (0°–90° sequence). As illustrated in Fig. 10a, the 3-dimensionally stacked scaffolds

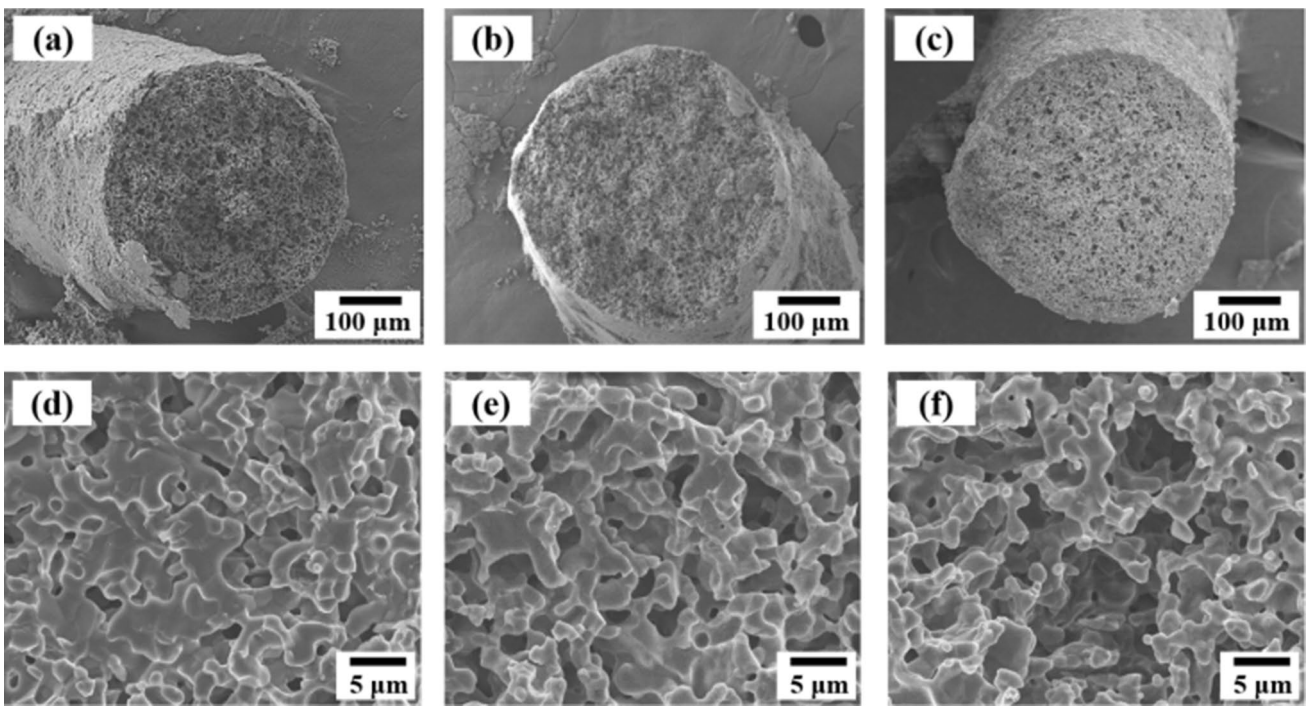

Fig. 9 Microstructure of sintered filaments fabricated through in situ UV curing-assisted 3D plotting with **a**, **d** 50 vol%, **b**, **e** 60 vol%, and **c**, **f** 70 vol% of terpene contents

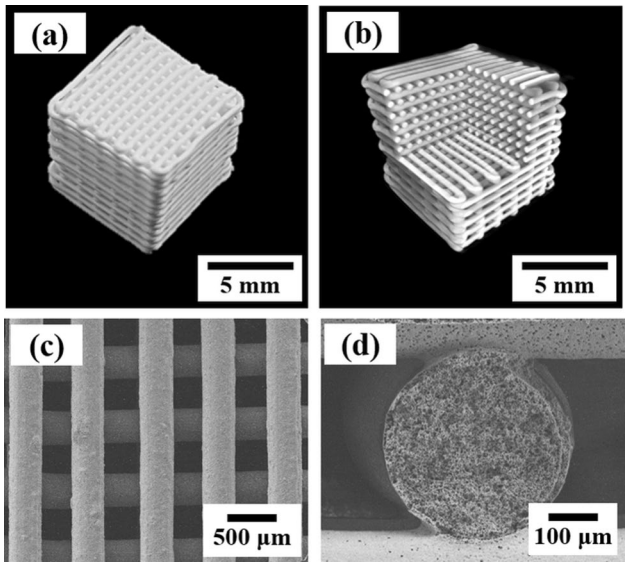

Fig. 10 **a** Typical optical image of sintered scaffolds produced by in situ UV curing-assisted 3D plotting, **b** reconstructed micro CT image, FE-SEM image of **c** top surface and **d** adhered part between the deposited layers produced by 60 vol% terpene filaments

were produced and notable delamination or deformations were not found after sintering at 1250 °C for 2 h. The measured sintering shrinkage, size of microchannel, and diameter of filament were similar. Further analysis on the structure was carried out with micro CT. In the Fig. 10b, internal macro-scale pores were proven to be well organized and the filaments were continuously connected. Adhesion between the layers, which is one of the critical points for additive manufacturing, was closely examined by SEM observation (Fig. 10c–d). As shown in Fig. 10c, transversely located BCP filaments with the diameter of ~ 350 µm were piled up following highly controlled path way. And circular shape of filament was preserved between the filaments, and three filaments were tightly bonded to one another (Fig. 10d). Overall porosity was measured as 71% and 84% with raising the terpene amounts from 50 to 70 vol% which was attributed to the enlarged microporosity even though the macroporosity of initial design was same.

One of the most remarkable aspects of suggested in situ UV curing-assisted 3D plotting is the shape retention ability of the filaments derived from photopolymerization. Figure 11 exhibits hierarchically constituted structure which consists of straight filaments between the lower filaments. In conventional ceramic additive manufacturing methods, supporting materials which are essential for creating complicated structure to hinder sagging of the filaments due to gravity. However, supporting materials should be eliminated since they are not originally necessary for final products. On the other hand, removal process of supporting materials requires considerable care and time not to damage the constructing filaments. In this respect, newly developed in situ UV curing-assisted 3D plotting technique is effective and useful to fabricate the ceramic products.

4 Conclusion and perspectives

In this paper, recently developed additive manufacturing methods for producing ceramic scaffolds with dual-scale pores which could facilitate specific functional abilities of each scaled pore were introduced. Based on the state of ceramic slurries, additive manufacturing techniques were categorized into lithography-based and extrusion-based systems. Both of the procedure exhibited excellent results which could be further employed in ceramic printing. However, there are some challenges which need to be improved for practical usage.

Mentioned lithography-based printing procedure utilized ceramic slurries with relatively high temperature which solidified at room temperature. However, preparation of ceramic slurries in elevated temperature causes fast evaporation of the freezing vehicles which could result in concentration gradient in the slurries during printing. Additionally, readily heated syringes and platform and heating system over the environment are needed to prevent solidification of the ceramic slurries. Thus, the advent of innovative ceramic slurries which could be mixed in liquid state at room temperature should be studied for further advancement.

In terms of the photocuring-assisted 3D plotting technique using frozen terpene feedstocks, highly porous ceramic scaffolds were successfully fabricated with dual-scale pores. And its unique self-supporting ability which overcome the limitation of traditional extrusion-based ceramic additive manufacturing methods could inspire broad range of applications. Even though the scaffolds consisted of macro-scale and micro-scale pores, body fluid could not rapidly infiltrate into the scaffold in physiological condition. Fabrication of hollow filaments by using additional material which are removable during post processing or heat treatment could induce penetration of body fluid into the scaffolds easier. And this would result in the improved bone to implant fixation.

The highest porosity of dual-scale porous ceramic products referred in this article was nearly 80% which for various fields. Still, there are increasing demands for ultra-high porosity which is around 90%. Even though using thinner struts could realize the ultra-high porosity, dramatically decrease mechanical properties would limit their usage. Therefore, incorporating and controlling micro-scale pores within the densified ceramic struts could achieve ultra-high porosity with less decreased mechanical properties.

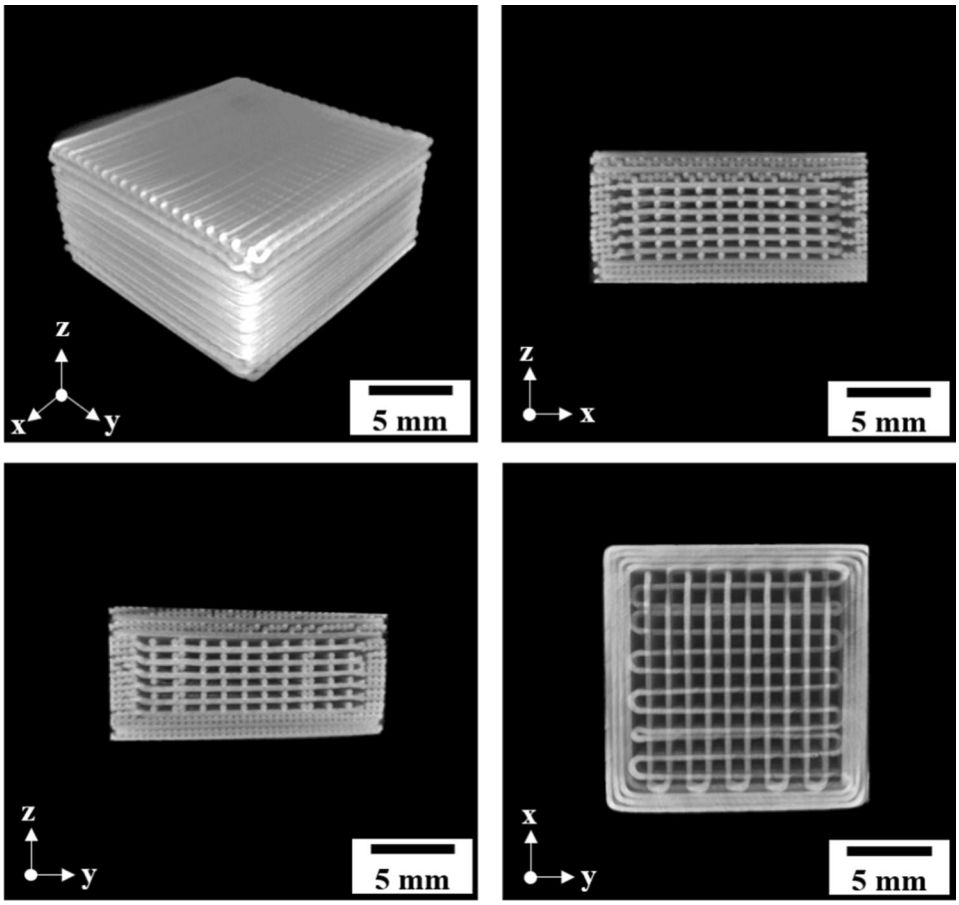

Fig. 11 Micro CT images of self-supporting structured products generated by in situ UV curing-assisted 3D plotting

Compliance with ethical standards

Conflict of interests The authors declare that they have no conflict of interest.

Ethical approval This article does not contain any studies with human participants or animals performed by the author.

References

1. Salyer KE, Hall CD. Porous hydroxyapatite as an onlay bone-graft substitute for maxillofacial surgery. Plast Reconstr Surg. 1989;84(2):236–44.
2. Tamai N, Myoui A, Tomita T, Nakase T, Tanaka J, Ochi T, Yoshikawa H. Novel hydroxyapatite ceramics with an interconnective porous structure exhibit superior osteoconduction in vivo. J Biomed Mater Res. 2002;59(1):110–7.
3. Boaro M, Vohs JM, Gorte RJ. Synthesis of highly porous yttria-stabilized zirconia by tape-casting methods. J Am Ceram Soc. 2003;86(3):395–400.
4. Myung J-H, Ko HJ, Im CH, Moon J, Hyun S-H. Development of solid oxide fuel cells (SOFCs) by tape-casting and single-step co-firing of monolithic laminates. Int J Hydrogen Energy. 2014;39(5):2313–9.
5. Grings Schmidt C, Hansen KK, Andersen KB, Fu Z, Roosen A, Kaiser A. Effect of pore formers on properties of tape cast porous sheets for electrochemical flue gas purification. J Eur Ceram Soc. 2016;36(3):645–53.
6. Li D, Li M. Porous Y2SiO5 ceramic with low thermal conductivity. J Mater Sci Technol. 2012;28(9):799–802.
7. Wu X, Ma H, Chen X, Li Z, Li J. Thermal conductivity and microstructure properties of porous SiC ceramic derived from silicon carbide powder. New J Glass Cer. 2013;03(01):43–7.
8. Fu K, Gong Y, Hitz GT, McOwen DW, Li Y, Xu S, Wen Y, Zhang L, Wang C, Pastel G, Dai J, Liu B, Xie H, Yao Y, Wachsman ED, Hu L. Three-dimensional bilayer garnet solid electrolyte based high energy density lithium metal–sulfur batteries. Energy Environ Sci. 2017;10(7):1568–75.
9. Han L, Deng X, Li F, Huang L, Pei Y, Dong L, Li S, Jia Q, Zhang H, Zhang S. Preparation of high strength porous mullite ceramics via combined foam-gelcasting and microwave heating. Ceram Int. 2018;44(12):14728–33.
10. Bruzauskaite I, Bironaite D, Bagdonas E, Bernotiene E. Scaffolds and cells for tissue regeneration: different scaffold pore sizes-different cell effects. Cytotechnology. 2016;68(3):355–69.
11. Sánchez-Salcedo S, Arcos D, Vallet-Regí M. Upgrading calcium phosphate scaffolds for tissue engineering applications. Key Eng Mater. 2008;377:19–42.
12. Loh QL, Choong C. Three-dimensional scaffolds for tissue engineering applications: role of porosity and pore size. Tissue Eng Part B Rev. 2013;19(6):485–502.
13. Li T, Zhai D, Ma B, Xue J, Zhao P, Chang J, Gelinsky M, Wu C. 3D printing of hot dog-like biomaterials with hierarchical architecture and distinct bioactivity. Adv Sci. 2019;6(19):1901146.

14. Deville S, Saiz E, Tomsia AP. Freeze casting of hydroxyapatite scaffolds for bone tissue engineering. Biomaterials. 2006;27(32):5480–9.
15. Ogden TA, Prisbrey M, Nelson I, Raeymaekers B, Naleway SE. Ultrasound freeze casting: fabricating bioinspired porous scaffolds through combining freeze casting and ultrasound directed self-assembly. Mater Des. 2019;164:1.
16. Fu Q, Rahaman MN, Dogan F, Bal BS. Freeze casting of porous hydroxyapatite scaffolds. I. Processing and general microstructure. J Biomed Mater Res B Appl Biomater. 2008;86:125–35.
17. Ji HB, Kim WY, Yang TY, Yoon SY, Kim BK, Park HC. Freeze casting of aqueous coal fly ash/alumina slurries for preparation of porous ceramics. J Phys Chem Solids. 2010;71(4):503–6.
18. Koh YH, Jun IK, Sun JJ, Kim HE. In situ fabrication of a dense/porous Bi-layered ceramic composite using freeze casting of a ceramic-camphene slurry. J Am Ceram Soc. 2006;89(2):763–6.
19. Lee H, Jang TS, Song J, Kim HE, Jung HD. The production of porous hydroxyapatite scaffolds with graded porosity by sequential freeze-casting. Mater (Basel). 2017;10(4):367.
20. Yook SW, Kim HE, Yoon BH, Soon YM, Koh YH. Improvement of compressive strength of porous hydroxyapatite scaffolds by adding polystyrene to camphene-based slurries. Mater Lett. 2009;63(11):955–8.
21. Choi HJ, Yang TY, Yoon SY, Kim BK, Park HC. Porous alumina/zirconia layered composites with unidirectional pore channels processed using a tertiary-butyl alcohol-based freeze casting. Mater Chem Phys. 2012;133(1):16–20.
22. Dong S, Zhu W, Gao X, Wang Z, Wang L, Wang X, Gao C. Preparation of tubular hierarchically porous silicate cement compacts via a tert-butyl alcohol (TBA)-based freeze casting method. Chem Eng J. 2016;295:530–41.
23. Song JH, Koh YH, Kim HE, Li LH, Bahn HJ. Fabrication of a porous bioactive glass-ceramic using room-temperature freeze casting. J Am Ceram Soc. 2006;89(8):2649–53.
24. Seong Y-J, Song E-H, Park C, Lee H, Kang I-G, Kim H-E, Jeong S-H. Porous calcium phosphate–collagen composite microspheres for effective growth factor delivery and bone tissue regeneration. Mater Sci Eng C 2020; 109.
25. Thijs I, Luyten J, Mullens S. Producing ceramic foams with hollow spheres. J Am Ceram Soc. 2004;87(1):170–2.
26. Tulliani JM, Lombardi M, Palmero P, Fornabaio M, Gibson LJ. Development and mechanical characterization of novel ceramic foams fabricated by gel-casting. J Eur Ceram Soc. 2013;33(9):1567–76.
27. Bhaskar S, Gyu Park J, Cho GH, Kim S, Kim IJ. Wet foam stability and tailoring microstructure of porous ceramics using polymer beads. Adv Appl Ceram 2015; 114(6):333–7.
28. Seitz H, Rieder W, Irsen S, Leukers B, Tille C. Three-dimensional printing of porous ceramic scaffolds for bone tissue engineering. J Biomed Mater Res B Appl Biomater 2005; 74(2):782–8.
29. Zhang B, Pei X, Song P, Sun H, Li H, Fan Y, Jiang Q, Zhou C, Zhang X. Porous bioceramics produced by inkjet 3D printing: effect of printing ink formulation on the ceramic macro and micro porous architectures control. Compos B Eng. 2018;155:112–21.
30. Michna S, Wu W, Lewis JA. Concentrated hydroxyapatite inks for direct-write assembly of 3-D periodic scaffolds. Biomaterials. 2005;26(28):5632–9.
31. Peng E, Wei X, Garbe U, Yu D, Edouard B, Liu A, Ding J. Robocasting of dense yttria-stabilized zirconia structures. J Mater Sci. 2017;53(1):247–73.
32. Nadkarni SS, Smay JE. Concentrated barium titanate colloidal gels prepared by bridging flocculation for use in solid freeform fabrication. J Am Ceram Soc. 2006;89(1):96–103.
33. Jo I-H, Ahn M-K, Moon Y-W, Koh Y-H, Kim H-E. Novel rapid direct deposition of ceramic paste for porous biphasic calcium phosphate (BCP) scaffolds with tightly controlled 3-D macrochannels. Ceram Int. 2014;40(7):11079–84.
34. Peng E, Wei X, Herng TS, Garbe U, Yu D, Ding J. Ferrite-based soft and hard magnetic structures by extrusion free-forming. RSC Adv. 2017;7(43):27128–38.
35. Yang S, Yang H, Chi X, Evans JRG, Thompson I, Cook RJ, Robinson P. Rapid prototyping of ceramic lattices for hard tissue scaffolds. Mater Des. 2008;29(9):1802–9.
36. Halloran JW. Ceramic stereolithography: additive manufacturing for ceramics by photopolymerization. Annu Rev Mater Res. 2016;46(1):19–40.
37. Lee YH, Lee JB, Maeng WY, Koh YH, Kim HE. Photocurable ceramic slurry using solid camphor as novel diluent for conventional digital light processing (DLP) process. J Eur Ceram Soc. 2019;39(14):4358–65.
38. Colombo P, Vakifahmetoglu C, Costacurta S. Fabrication of ceramic components with hierarchical porosity. J Mater Sci. 2010;45(20):5425–55.
39. Wegst UG, Bai H, Saiz E, Tomsia AP, Ritchie RO. Bioinspired structural materials. Nat Mater. 2015;14(1):23–36.
40. Zhang K, Fan Y, Dunne N, Li X. Effect of microporosity on scaffolds for bone tissue engineering. Regen Biomater. 2018;5(2):115–24.
41. Cho YS, Lee JS, Hong MW, Lee S-H, Kim YY, Cho Y-S. Comparative assessment of the ability of dual-pore structure and hydroxyapatite to enhance the proliferation of osteoblast-like cells in well-interconnected scaffolds. Int J Pr Eng Man. 2018;19(4):605–12.
42. Tomeckova V, Halloran JW. Porous ceramics by photopolymerization with terpene-acrylate vehicles. J Am Ceram Soc. 2012;95(12):3763–8.
43. Tomeckova V, Halloran JW. Macroporous polyacrylates from terpene-acrylate thermoreversible photopolymerizable vehicle. J Mater Sci. 2012;47(16):6166–78.
44. Maeng W-Y, Jeon J-W, Lee J-B, Lee H, Koh Y-H, Kim H-E. Photocurable ceramic/monomer feedstocks containing terpene crystals as sublimable porogen for UV curing-assisted 3D plotting. J Eur Ceram Soc. 2020;40(9):3469–77.
45. Muth JT, Dixon PG, Woish L, Gibson LJ, Lewis JA. Architected cellular ceramics with tailored stiffness via direct foam writing. Proc Natl Acad Sci USA. 2017;114(8):1832–7.
46. Zhang X, Zhang Y, Lu Y, Zhang S, Yang J. Hierarchically porous ceria with tunable pore structure from particle-stabilized foams. J Eur Ceram Soc. 2020;40(12):4366–72.
47. Zhang X, Huo W, Liu J, Zhang Y, Zhang S, Yang J. 3D printing boehmite gel foams into lightweight porous ceramics with hierarchical pore structure. J Eur Ceram Soc. 2020;40(3):930–4.
48. Zocca A, Elsayed H, Bernardo E, Gomes CM, Lopez-Heredia MA, Knabe C, Colombo P, Gunster J. 3D-printed silicate porous bioceramics using a non-sacrificial preceramic polymer binder. Biofabrication. 2015;7(2):025008.
49. Moon YW, Shin KH, Koh YH, Jung HD, Kim HE. Three-dimensional ceramic/camphene-based coextrusion for unidirectionally macrochanneled alumina ceramics with controlled porous walls. J Am Ceram Soc. 2014;97(1):32–4.
50. Moon YW, Choi IJ, Koh YH, Kim HE. Macroporous alumina scaffolds consisting of highly microporous hollow filaments using three-dimensional ceramic/camphene-based co-extrusion. J Eur Ceram Soc. 2015;35(16):4623–7.
51. Lee LB, Maeng WY, Koh YH, Kim HE. Novel additive manufacturing of photocurable ceramic slurry containing freezing vehicle as porogen for hierarchical porous structure. Ceram Int. 2019;45(17):21321–7.
52. Kim JW, Lee JB, Koh YH, Kim HE. Digital light processing of freeze-cast ceramic layers for macroporous calcium phosphate

scaffolds with tailored microporous frameworks. Materials (Basel). 2019; 12(18).
53. Nishihora RK, Rachadel PL, Quadri MGN, Hotza D. Manufacturing porous ceramic materials by tape casting-a review. J Eur Ceram Soc. 2018;38(4):988–1001.
54. Ren L, Zeng Y-P, Jiang D. Fabrication of gradient pore TiO_2 sheets by a novel freeze? Tape-casting process. J Am Ceram Soc. 2007;90(9):3001–4.
55. Leu MC, Deuser BK, Tang L, Landers RG, Hilmas GE, Watts JL. Freeze-form extrusion fabrication of functionally graded materials. CIRP Ann. 2012;61(1):223–6.
56. Tang SY, Yang L, Li GJ, Liu XW, Fan ZT. 3D printing of highly-loaded slurries via layered extrusion forming: parameters optimization and control. Addit Manuf. 2019;28:546–53.
57. Cui H, Hensleigh R, Yao D, Maurya D, Kumar P, Kang MG, Priya S, Zheng XR. Three-dimensional printing of piezoelectric materials with designed anisotropy and directional response. Nat Mater. 2019;18(3):234–41.
58. Dehurtevent M, Robberecht L, Hornez JC, Thuault A, Deveaux E, Behin P. Stereolithography: a new method for processing dental ceramics by additive computer-aided manufacturing. Dent Mater. 2017;33(5):477–85.
59. Maeng WY, Lee JB, Koh YH, Kim HE. Innovative in situ photocuring-assisted 3D plotting technique for complex-shaped ceramic architectures with high shape retention. Ceram Int. 2019;45(7):8440–7.
60. Kapfer SC, Hyde ST, Mecke K, Arns CH, Schroder-Turk GE. Minimal surface scaffold designs for tissue engineering. Biomaterials. 2011;32(29):6875–82.
61. Almeida HA, Bartolo PJ. Design of tissue engineering scaffolds based on hyperbolic surfaces: structural numerical evaluation. Med Eng Phys. 2014;36(8):1033–40.
62. Campion CR, Chander C, Buckland T, Hing K. Increasing strut porosity in silicate-substituted calcium-phosphate bone graft substitutes enhances osteogenesis. J Biomed Mater Res B Appl Biomater 2011; 97(2):245–54.
63. Rustom LE, Boudou T, Lou S, Pignot-Paintrand I, Nemke BW, Lu Y, Markel MD, Picart C, Johnson AJW. Micropore-induced capillarity enhances bone distribution in vivo in biphasic calcium phosphate scaffolds. Acta Biomater. 2016;44:144–54.
64. Baek J, Lee H, Jang TS, Song JH, Kim HE, Jung HD. Incorporation of calcium sulfate dihydrate into hydroxyapatite microspheres to improve the release of bone morphogenetic protein-2 and accelerate bone regeneration. ACS Biomater Sci Eng. 2018;4(3):846–56.
65. Moon YW, Choi IJ, Koh YH, Kim HE. Porous alumina ceramic scaffolds with biomimetic macro/micro-porous structure using three-dimensional (3-D) ceramic/camphene-based extrusion. Ceram Int. 2015;41(9):12371–7.
66. Ahn MK, Moon YW, Maeng WY, Koh YH, Kim HE. Design and production of continuously gradient macro/microporous calcium phosphate (CaP) scaffolds using ceramic/camphene-based 3D extrusion. Mater (Basel). 2017; 10(7).